Power Electronics and Drives
Volume 11(46), 2026 DOI: 10.2478/pead-2026-0019

Detection of Rotor Unbalance in Multi-Mass Systems Using FFT and Bispectrum

Research paper

Paweł Ewert[1,*], Bartłomiej Wicher[2], Tomasz Pajchrowski[2]

[1]*Department of Electrical Machines, Drives and Measurements, Wroclaw University of Science and Technology, Wybrzeze Wyspianskiego 27, 50-370 Wroclaw, Poland*
[2]*Institute of Robotics and Machine Intelligence, Poznań University of Technology, ul. Piotrowo 3A, 60-965 Poznań, Poland*

Received: 9 March, 2026; Received in the revised form: 11 May, 2026; Accepted: 26 May, 2026

Abstract: Unbalance of rotating components is a highly destructive phenomenon that adversely affects the operation of a machine. Vibrations generated by an unbalanced rotor are transmitted through the bearing assembly to the machine housing, accelerating the ageing process of the bearings and, over time, leading to their premature failure. Unfortunately, there are no instruments that allow unbalance to be detected directly during machine operation, which makes it necessary to monitor its secondary effects. An additional factor that complicates the detection of unbalance is the coupling of the motor with the driven machine. The method of connecting the two machines is also significant. The article discusses selected methods for detecting rotor unbalance in single-mass and two-mass systems with elastic coupling. The adopted mathematical models based on gravitational force and centrifugal force are presented. The laboratory test stand and research methodology are also described. To model the unbalance, a test mass is added to the disc rotating on the motor shaft. The added mass constituted less than 0.5% of the mass of the rotating components. Tests were conducted in steady-state conditions at a speed below 20% of the motor's rated speed. The study analysed mechanical vibrations and the reference current from the control system. Fast Fourier transform and higher-order bispectrum analysis were used to obtain diagnostic symptoms.

Keywords: *unbalance • two – mass system • FFT • bispectrum*

1. Introduction

Unbalance is a phenomenon inherently linked to the operation of rotating components, especially those found in electric machine rotors. The mechanical vibrations produced by an unbalanced rotor propagate through the machine's housing, leading to reduced durability and decreased operational reliability. Minimising the adverse effects of this issue on the performance of the entire drive system requires early detection of the initial stages of damage. Modern diagnostic methods enable the identification of a wide range of faults that may occur in electrical machines, including primarily mechanical faults (such as rolling bearing wear, misalignment, eccentricity, or unbalance of rotating parts), electrical faults (including, among others, inter-turn short circuits in stator windings and rotor cage damage), as well as magnetic faults related, for example, to demagnetisation processes in permanent-magnet motors (Chen et al., 2019; Krichen et al., 2017; Orlowska-Kowalska et al., 2022; Wang et al., 2014). Mechanical damage to a permanent magnet (e.g., chipping) may cause rotor unbalance and irregularities in the airgap magnetic field. This results in increased pulsations of electromagnetic torque, vibration levels, and noise; therefore, diagnostic methods combining the analysis of mechanical vibration and electrical signals are increasingly used (Calderon-Uribe et al., 2023; Rahman and Uddin, 2017), enabling more effective detection of rotor unbalance at an early stage of its development.

* *Email: pawel.ewert@pwr.edu.pl*

The purpose of diagnostic systems is to detect damage as quickly as possible, allowing the user to plan the necessary repair in advance and avoid costly downtime. Currently, both ready-made industrial diagnostic systems and solutions built in-house using widely available measurement cards and sensors are available, enabling flexible adaptation to the needs of a facility. The latter approach also makes it possible to integrate additional functions, such as artificial intelligence algorithms for automatic classification of operating states and fault prediction (Boudiaf et al., 2018; Ewert et al., 2020; Wolkiewicz and Skowron, 2017). Diagnostic systems are most often based on the analysis of signals, such as current, mechanical vibrations, or noise, and their effectiveness depends not only on the quality of the measurement hardware but also on the applied data processing and analysis methods (Nandi et al., 2005; Niu et al., 2023). Modern approaches also include deep machine learning techniques and data fusion from multiple sensors, which significantly improve the quality of fault detection and classification in rotating machines (e.g., vibration analysis and machine learning techniques in rotating machinery diagnostics) (Tiboni et al., 2022; Tran et al., 2022).

Each diagnostic signal contains symptoms of various faults. Diagnostic systems may detect single faults or identify multiple types of failure. In Ebrahimi et al. (2009), based on the fast fourier transform (FFT) analysis of mechanical vibrations, three distinct faults were identified: broken rotor cage bars, rotor eccentricity, and a damaged rolling bearing. Vibration analysis also makes it possible to detect rotor unbalance. By using mean, maximum, and root mean square (RMS) values, along with additional statistical indicators, such as skewness, kurtosis, and the crest factor, the study (Ribeiro Junior et al., 2020b) demonstrated the possibility of identifying rotor unbalance, rotor cage damage, and rolling bearing failures. Additionally, methods based on the wavelet transform allow precise localisation of signal changes associated with the development of faults, improving early failure detection (Ruqiang et al., 2014). Time–frequency analysis makes it possible to distinguish simultaneous defects in different rotor components, such as eccentricity and unbalance (Jia et al., 2022). Modern approaches also include the use of statistical indicators and signal entropy, which increases the accuracy of fault classification in electrical machines (Zhang and Wang, 2019).

The stator current can be successfully used to detect electrical faults (Diversi et al., 2025; Thomson and Fenger, 2001). In Liang et al. (2018), the application of stator current and mechanical vibration analysis for detecting short-circuit faults in PMSM stator windings is shown. The study demonstrates the ability to detect rotor unbalance in an induction motor supplied by a frequency converter, using FFT and bispectrum analysis of stator current and vibration acceleration signals, as demonstrated in Ewert (2020); Ewert et al. (2022). In Yatsugi et al. (2023), a method is presented to detect and classify various types of induction motor faults based on the characteristics of the stator current signal. Meanwhile, in Thang et al. (2020), the stator current signal under frequency converter supply conditions enables identification of rotor and stator defects. The above research results confirm that the stator current signal contains significant diagnostic information in the case of both mechanical and electrical faults. Moreover, the application of higher-order analyses enables more effective differentiation of rotor unbalance from other defects occurring under frequency converter supply conditions (Thang et al., 2020; Thomson and Fenger, 2001).

In drive system diagnostics, the selection of an appropriate diagnostic signal is crucial, as is the method used to process it. The literature presents a wide spectrum of signal processing techniques used in the diagnostics of electrical machines. Advanced time–frequency analysis methods are gaining increasing interest (Ewert et al., 2024), as are approaches based on multiscale transforms (Tran et al., 2022), which enable effective extraction of fault symptoms from non-stationary and non-linear signals. In addition, solutions are described that integrate classical signal analysis methods with intelligent classification algorithms, significantly increasing the reliability of identifying various types of defects (Jia et al., 2022; Łuczak, 2024; Orhan et al., 2025). A review of current diagnostic techniques used in permanent magnet synchronous motors, including time–frequency methods, magnetic flux monitoring, and advanced signal analyses, is presented in Sergakis et al. (2025), while a detailed literature analysis in the field of permanent magnet motor diagnostics is provided in Dogan and Tetik, (2021); Orlowska-Kowalska et al. (2022).

The modelling of unbalance can be realised in several ways. A test mass can be mounted, for example, directly on the rotor, on an additional disc fitted to the motor shaft, or on the motor fan. Moreover, the issue of unbalance concerns various types of electrical machines, which makes its early detection crucial for the reliable and safe operation of drive systems. The literature indicates that an appropriate method to represent unbalance allows for a reliable assessment of the effectiveness of diagnostic methods and the comparison of experimental results with theoretical models. For example, in Ewert, (2020), a method for detecting rotor unbalance in a drive system is presented based on the analysis of mechanical vibration signals and electrical quantities, taking into account

frequency converter supply. In Faiz et al. (2017), static and dynamic eccentricity diagnostic methods in electrical machines were analysed, based on modelling the phenomenon and examining characteristic symptoms in diagnostic signals. Particular attention is given to multi-mass systems with long shafts, where unbalance can lead to complex dynamic phenomena and an increase in torsional vibration amplitudes (Ewert et al., 2024; Sergakis et al., 2025).

This work therefore concentrates on the detection of unbalance in a two-mass, long-shaft system incorporating two brushless AC servomotors. Special attention is given to multi-mass systems with long shafts, where unbalance can lead to complex dynamic phenomena, including an increase in torsional vibration amplitudes and couplings between individual masses. In such structures, unbalance of a single component can affect the dynamic response of the entire system, which significantly complicates its unambiguous identification.

To detect rotor unbalance, FFT and bispectrum analyses were applied to the mechanical vibration acceleration signal and to the speed controller's reference current, enabling the evaluation of both linear and non-linear relationships between the measured quantities. Unbalance was introduced by attaching additional test masses to a rotating disc rigidly coupled to the motor shaft—an approach commonly used in experimental diagnostics of rotating machinery, as it allows for controlled excitation of dynamic disturbances.

2. Description of the Unbalance of Rotating Elements

Unbalance occurs when a rotating element with an asymmetrical distribution of mass in relation to its rotational centre is set in motion. The result of unbalance are additional centrifugal forces and moments, which adversely affect the bearings. In fact, they contribute to increased mechanical vibrations and noise (AbdulBary et al., 2021).

According to Figure 1, the introduction of an additional test mass m « M mounted at an angle α at a distance of $\vec{r}$ from the axis of rotation O of a cylinder with mass M and moment of inertia J causes the shift of the centre of gravity of the rotating element from point O to point O_m by the vector $\vec{r_m}$. This vector is referred to as the eccentricity of the centre of gravity (Yamamoto et al., 2016). In this case, unequal balance (unbalance) is defined as the product of the testing mass m and the vector $\vec{r}$ on which it is installed (1) (Yamamoto et al., 2016):

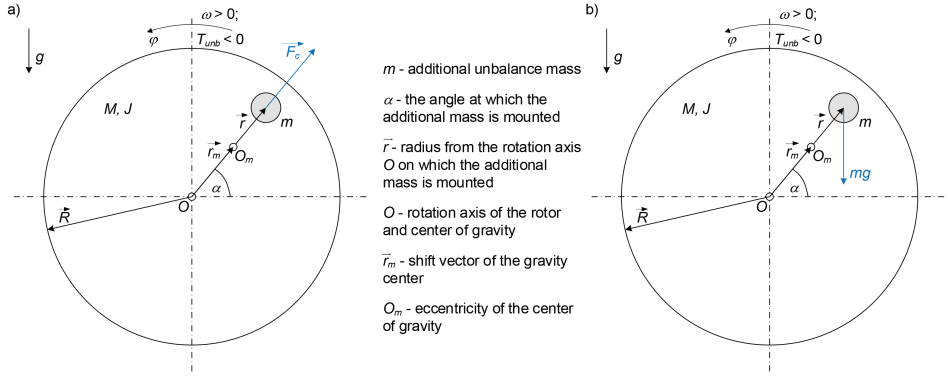

Figure 1. Graphical illustration of rotor unbalance, (a) generation of centrifugal force, (b) generation of a moment of force.

$$\vec{N} = m\vec{r} \tag{1}$$

As shown in Figure 1a, setting the element with the additional test mass m into rotational motion at angular velocity ω generates a centrifugal force $\vec{F_c}$ (2) (Yamamoto et al., 2016):

$$\vec{F_c} = m\vec{r}\omega^2 \tag{2}$$

The cause of the increase in vibration levels is the presence of an unbalanced centrifugal force exerted on the machine housing. Since the unbalance depends on the angular velocity ω an increase in the amplitude at the rotational frequency can be observed in the mechanical vibration spectrum (3) (Korkua et al., 2010):

$$f_{\text{unb}} = f_r = \frac{\omega}{2\pi} = \frac{n}{60} \tag{3}$$

where f_{unb} is the fault frequency that indicates the occurrence of rotor unbalance, f_r is the rotational frequency of the rotor, and n its rotational speed.

The second approach considered (Figure 1b) involves analysing the effect of an additional test mass m on the generation of torque caused by gravitational interaction (4) (Ewert et al., 2024; Kim, 2009). In this case, centrifugal force is not included in the control system. The torque acting on the test mass m can be expressed by the following formula:

$$T_{\text{unb}} = J\frac{d\omega}{dt} = mgr\cos(\varphi) \tag{4}$$

where φ is the angle of rotation.

If we assume that the rotating element is a cylinder with mass M and radius R, then the angular acceleration resulting from the unbalance caused by the test mass m is a cosine function of the angle and is directly proportional to the magnitude of the unbalance (4). During rotation, there is an additional component of angular acceleration that is directly related to the test mass and the instantaneous angular velocity ω (5):

$$\frac{d\omega}{dt} = \frac{mgr}{0,5MR^2}\cos(\varphi) = \frac{mgr}{0,5MR^2}\cos(\omega t) \tag{5}$$

Due to the small value of the mass m relative to the mass M of the rotating element, this acceleration will have a small amplitude. The disturbance generated by the unbalance should be compensated for by the speed-control system, which should be visible as an additional component of the active current at angular velocity ω in the control signal. Therefore, both in the mechanical vibration acceleration signal and in the control signal, the additional component described by Eq. (3) should be sought.

3. Fundamental Concepts of the Bispectrum Transform

The bispectrum is a higher-order transform which, unlike the power spectrum, does not lose information about the phase shift of the analysed signals (Hachemi Benbouzid, 2000). Its advantage lies in its ability to improve the signal-to-noise ratio, which can be particularly important when analysing symptoms with relatively small amplitudes (Sun et al., 2019). The bispectrum of two variables (f_1 and f_2) is expressed as the product of the Fourier transforms (6) $X(f)$ of a single variable (Argenti et al., 2011; Matsuoka and Ulrych, 1984):

$$B_3(f_1, f_2) = X(f_1)X(f_2)X^*(f_1 + f_2) \tag{6}$$

where:

$X^*()$ denotes the complex conjugate,

$$0 \le f_1 \le f_2 \le \frac{f_s}{2}, f_1 + f_2 \le \frac{f_s}{2}.$$

f_s – sampling frequency.

From a computational point of view, a characteristic feature of the bispectrum is the symmetry of its arguments, which means that changing their order does not affect the calculated value. (Matsuoka and Ulrych, 1984). The most important symmetries of the bispectrum are (7) (Argenti et al., 2011; Matsuoka and Ulrych, 1984; Sun et al., 2019):

$$B_3(f_1,f_2)=B_3(f_2,f_1)=B_3(-f_2,-f_1)=$$
$$=B_3(f_1,-f_1-f_2)=B_3(-f_1-f_2,f_2)=$$
$$=B_3(-f_1-f_2,f_1)=B_3(f_2,-f_1-f_2) \tag{7}$$

Due to the above relationship, the calculations can be limited to a single region, called the principal domain (Region I) (Schmidt, 2020), shown in Figure 2.

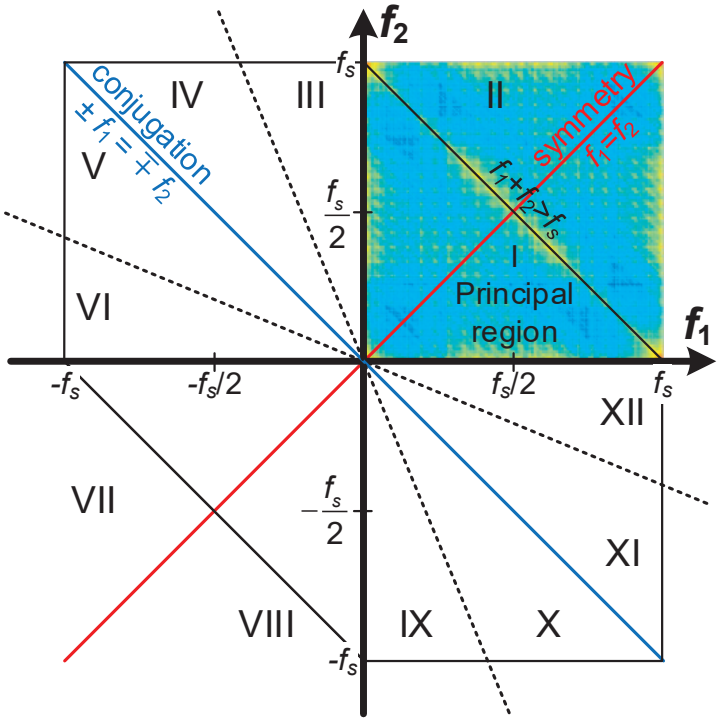

Figure 2. The principal domain and symmetry regions of the bispectrum.

4. Laboratory Setup and Research Methods

Laboratory tests were performed on a dual-mass system which consisted of two permanent magnet synchronous motors (PMSM) (Brushless AC Servomotor 95UMB301CASAA Control Techniques Unimotor) with a rated power of 3 kW, three pairs of poles, and a rotational speed of 3000 rpm. The elastic element connecting the two motors was a long shaft of 6 mm diameter. A disc is installed in the tested motor, in which the test masses are installed with a radius of 42 mm. To minimise mechanical vibrations generated during operation, the drive system is fixed on a concrete foundation. Figure 3 shows a photograph of the laboratory setup of the tested drive system with an elastic coupling, which allows for the modelling of rotor unbalance. The mechanical structure of the test stand did not include any adjustment elements; in particular, there was no possibility of aligning its components, and no preliminary balancing procedure was performed. Consequently, even before the addition of the test masses, the system could exhibit, and indeed exhibited, characteristics typical of an unbalanced and misaligned mechanical system.

During the experiments, mechanical vibration acceleration is recorded using a National Instruments NI-9234 data acquisition card. Mechanical vibrations were measured with a type 4506 three-axis piezoelectric accelerometer type 4506 from Brüel & Kjaer, mounted on the motor's mounting bracket. The reference current I_{qREF} and the motor angular velocity ω_{motor} were recorded using a NI USB-9215 data acquisition card. All signals were recorded for 10 s with a sampling frequency of 12.8 kS/s. The current I_{qREF} is generated by a vector control system implemented on an Analog Devices SHARC DSP 26369 signal processor. The motor is powered by a laboratory three-phase inverter.

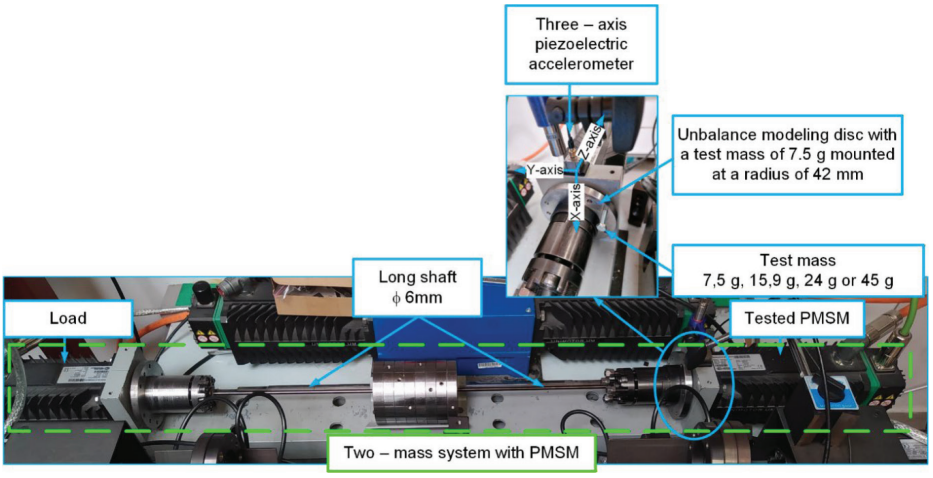

Figure 3. Photograph of laboratory stand for unbalance research in two-mass system. PMSM, permanent magnet synchronous motors.

Rotor unbalance is modelled using four test masses: 7.5 g, 15.9 g, 24 g, and 45 g. The tested drive system operated without load at a constant angular velocity of 60 rad/s. Two cases were investigated. In the first, the influence of the test mass on the operation of the single motor (single-mass system) is assessed, while in the second, the effect of the same unbalance on the operation of the two-mass system with an elastic coupling is examined. All experiments were conducted under steady-state conditions.

The motor tested operated within the control system as shown in Figure 4, which included two feedback loops: an inner current regulation loop and an outer speed regulation loop with an active disturbance rejection control (ADRC) controller (Wicher and Nowopolski, 2017). During laboratory experiments, the parameters of the speed and current control loops were not modified.

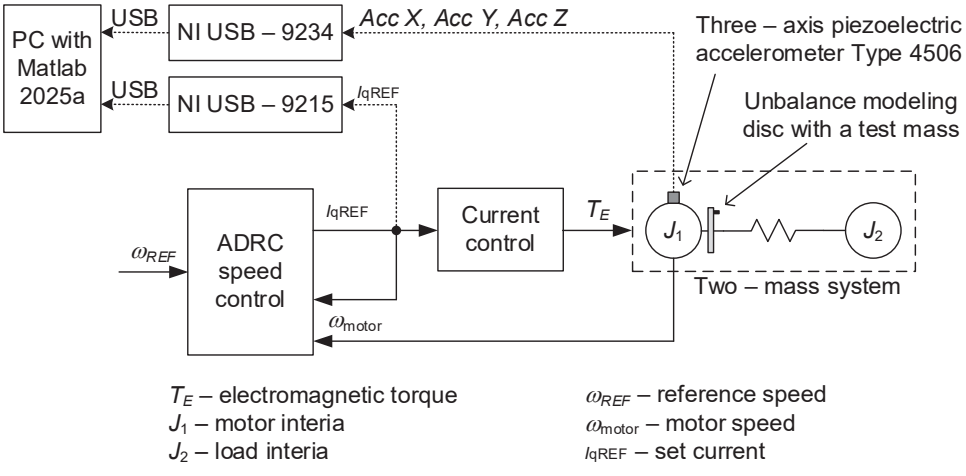

Figure 4. Block diagram of the control system including modules for measuring current and mechanical vibration acceleration.

4.1. Preliminary assumptions

The use of a triaxial piezoelectric accelerometer enabled simultaneous measurement of mechanical vibration acceleration in three axes: radial (*X*-axis), tangential (*Y*-axis), and axial (*Z*-axis). Preliminary analysis of the measured signals showed that in the radial direction, vibrations were effectively damped by the massive concrete foundation on which the drive system is mounted. In the axial direction, the introduction of a long shaft-shaped mechanical coupling adversely affected the measured signal. These disturbances significantly hindered the detection of unbalance symptoms. Only in the tangential direction (*Y*-axis) were unbalance symptoms visible in the mechanical vibration acceleration signal for both the single-mass motor system and the two-mass drive system.

The use of a high sampling rate for the recorded signals (12.8 kS/s) had a negative impact on the computation time of the bispectrum transform (from several dozen seconds to several minutes). Based on the conducted tests, the sampling rate of the recorded signals was reduced to 200 S/s without changing the recording duration. The applied resampling process did not affect the resolution of the bispectrum or FFT transforms but instead reduced the computation time to several dozen seconds. Moreover, the analysed frequencies were within the range up to 30 Hz, that is, below the Nyquist frequency, which after resampling was 100 Hz.

The configuration parameters of the bispectrum transform used are listed in Table 1.

Table 1. Summary of parameters in the bispectrum analysis.

Bispectrum parameters	Value/method
Bispectrum estimator	Direct FFT (Direct FFT-based averaged segment method)
Segment length	2000
Overlap	50%
Window type	Hamming
Averaging/smoothing strategy	Ensemble averaging
Scaling/normalisation	Raw bispectrum

The most significant differences occurred in the signals measured for the single-mass and two-mass systems. The introduction of an elastic coupling increased the background level of the measured signals and contributed to higher amplitudes of the analysed frequencies. Figure 5 presents three-dimensional bispectra of vibration acceleration measured along the *Y*-axis for the single-mass system (Figure 5a) and the two-mass system (Figure 5b). The presented bispectra correspond to an electric drive with an installed test mass of 45 g. To facilitate comparison of both cases, identical axis ranges were used in the figures. Due to the range of the analysed symptoms (up to ($3f_r$, $3f_r$) ≈ (29 Hz, 29 Hz)), the bispectra shown in Figures 5 and 6 were limited to 45 Hz.

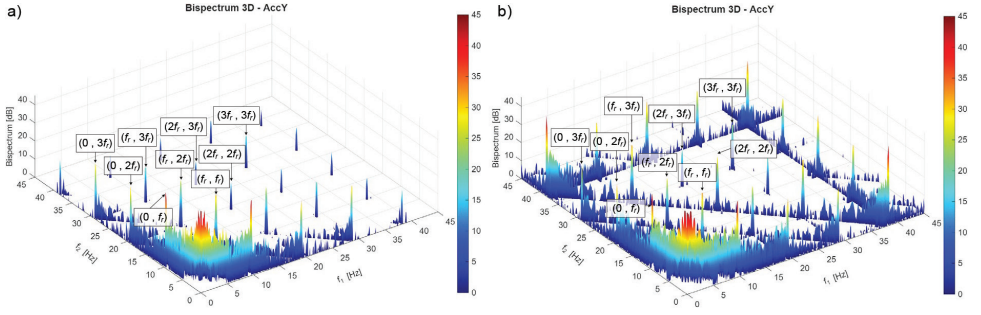

Figure 5. Three-dimensional bispectra of mechanical vibration acceleration signal measured along the *Y*-axis of the drive with an installed test mass of 45 g: (a) single-mass system, (b) two-mass system.

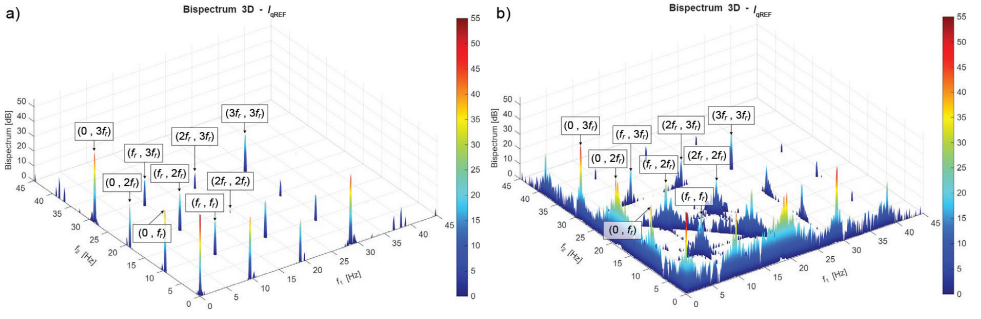

Figure 6. Three-dimensional bispectra of the I_{qREF} current signal of the drive with an installed test mass of 45 g: (a) single-mass system, (b) two-mass system.

A similar comparison was performed for the I_{qREF} current. Figure 6a presents the three-dimensional bispectrum of the current measured for the single-mass system with an installed test mass of 45 g. The presented bispectrum is free from disturbances that are visible in the two-mass system (Figure 6b). To facilitate the interpretation of the three-dimensional plots, identical ranges were set for each axis.

Despite the occurring disturbances, the symptoms indicating the presence of rotor unbalance are visible in the presented figures. To assess the usefulness of the individual symptoms for detecting rotor unbalance, they were subjected to detailed analysis, which is presented in Chapter 5.

5. Laboratory Test Results

5.1. The influence of mass for the single-mass system

As part of the study, two signal processing methods were evaluated. The first was the classical FFT analysis, and the second was the higher-order bispectrum transform. The purpose of applying the bispectrum transform was to determine whether it would provide a greater number of symptoms indicating rotor unbalance.

Figure 7 shows a comparison of the amplitude increase of three symptoms (kf_r, where k = 1, 2, 3) derived from the FFT analysis of mechanical vibration acceleration measured in the *Y*-axis direction (Figure 3). To ensure consistency across all comparisons presented in the paper, the analysis was performed using a decibel scale.

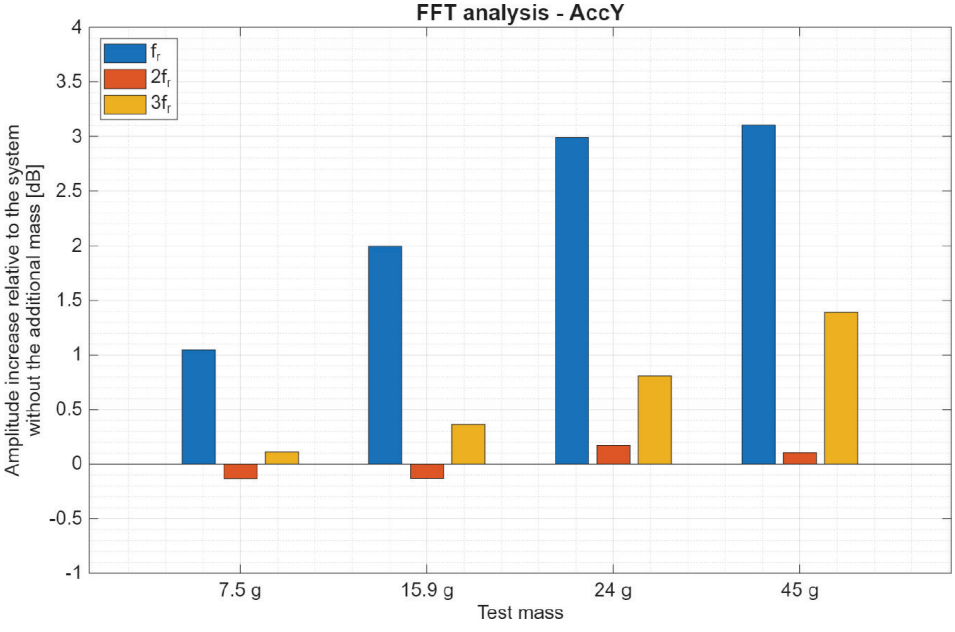

Figure 7. Summary of changes in the amplitude of kf_r symptoms derived from the spectrum of mechanical vibration acceleration.

Based on the analysis of the drawing, it can be concluded that the rotational frequency f_r, whose amplitude increased by approximately 3 dB after adding a test mass of 24 g, is the most effective symptom for detecting rotor unbalance based on FFT analysis of mechanical vibration acceleration. Increasing the test mass to 45 g did not result in a significant increase in the amplitude of the analysed symptom. The occurrence of unbalance is also visible in the change in amplitude of the $3f_r$ frequency; however, in this case, the change is approximately 1.4 dB.

Figure 8 shows a comparison of the changes in the amplitudes of the characteristic frequencies (kf_r, kf_r) obtained from the bispectrum analysis of mechanical vibration acceleration measured along the *Y*-axis.

The analysis of the figure indicates that there are four symptoms that can be used to detect rotor unbalance in the tested motor. The smallest amplitude increases after adding a 45 g test mass were observed for the (0, f_r) and (f_r, f_r) symptoms, amounting to approximately 2.8 dB and 3.1 dB, respectively. The largest amplitude increases were recorded for the (f_r, $3f_r$) and ($2f_r$, $2f_r$) symptoms, reaching approximately 13.1 dB and 10.9 dB, respectively.

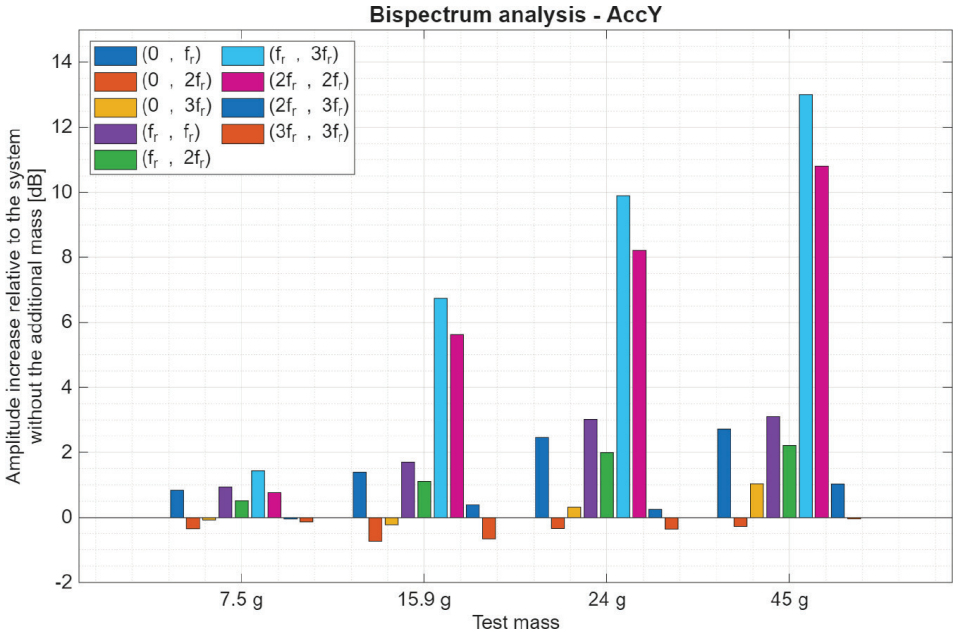

Figure 8. Summary of changes the amplitudes of characteristic symptoms (kf_r, kf_r) derived from the bispectral analysis of mechanical vibration acceleration.

Figure 9 shows only the positive difference in the amplitude of the symptoms (kf_r, kf_r) obtained from the bispectral analysis of vibration acceleration for the motor without an installed test mass and with an installed test mass of m = 45 g. Figure 9 is a three-dimensional representation of the selected data shown in Figure 8. The data used to generate all the comparisons presented in the article were obtained by searching for the characteristic amplitudes of the symptoms directly from the results of the bispectrum analysis.

The second signal analysed was the I_{qREF} current, which was also subjected to FFT analysis (Figure 10) and bispectrum analysis (Figure 11). Based on the FFT analysis, only one symptom could be identified for detecting rotor unbalance. The amplitude increase of the rotational frequency for a test mass of 45 g is approximately 3.4 dB.

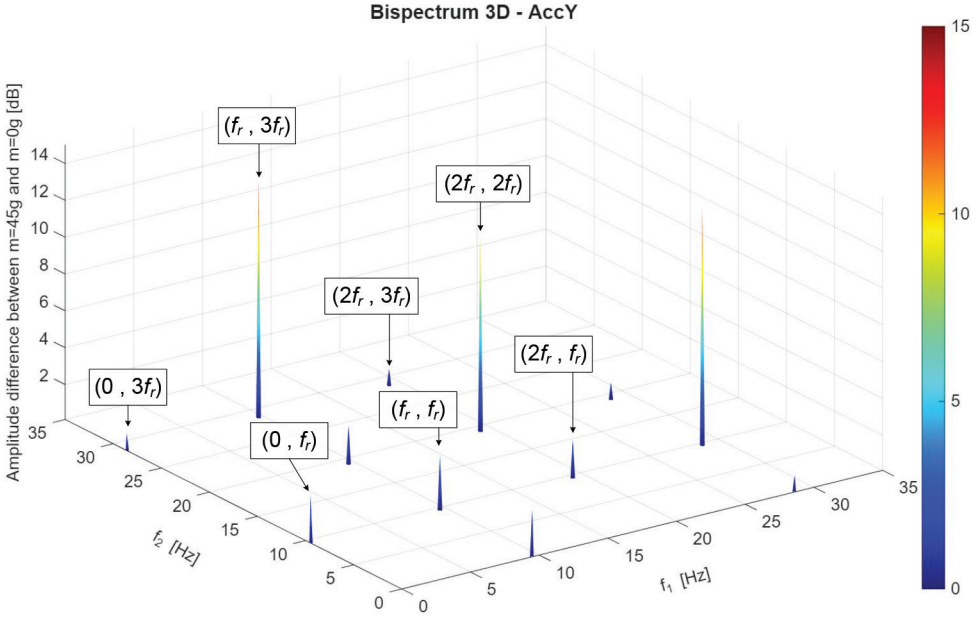

Figure 9. Difference between the amplitudes of the symptoms (kf_r, kf_r) derived from the bispectral analysis of mechanical vibration acceleration for the motor without an installed test mass (m = 0 g) and an installed test mass m = 45 g.

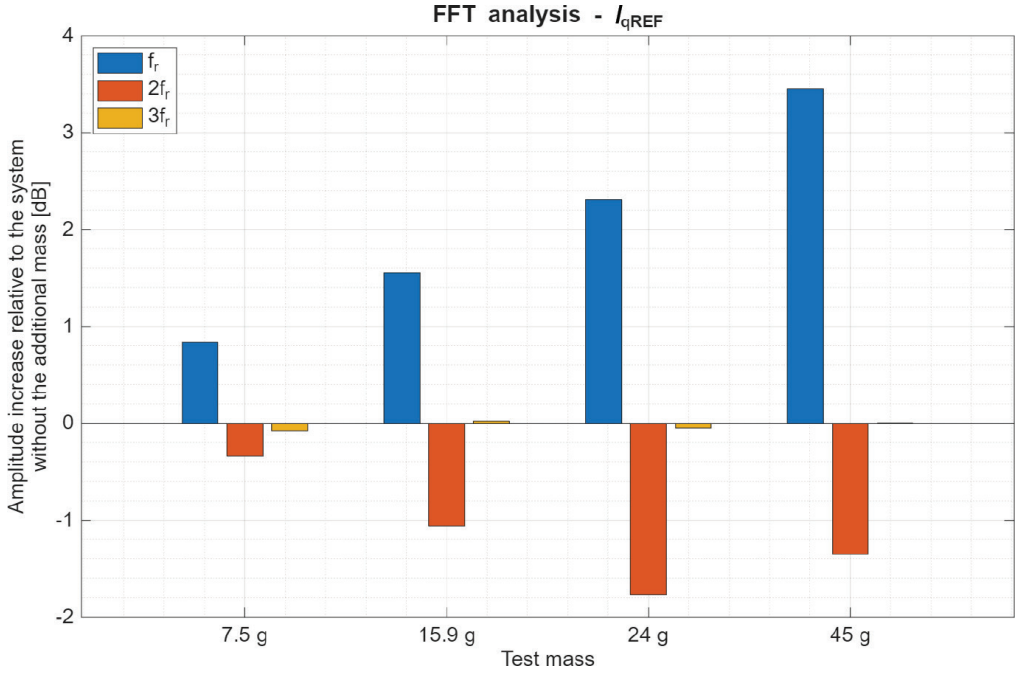

Figure 10. Summary of changes in the amplitude of kf_r symptoms derived from the spectrum of the I_{qREF} current.

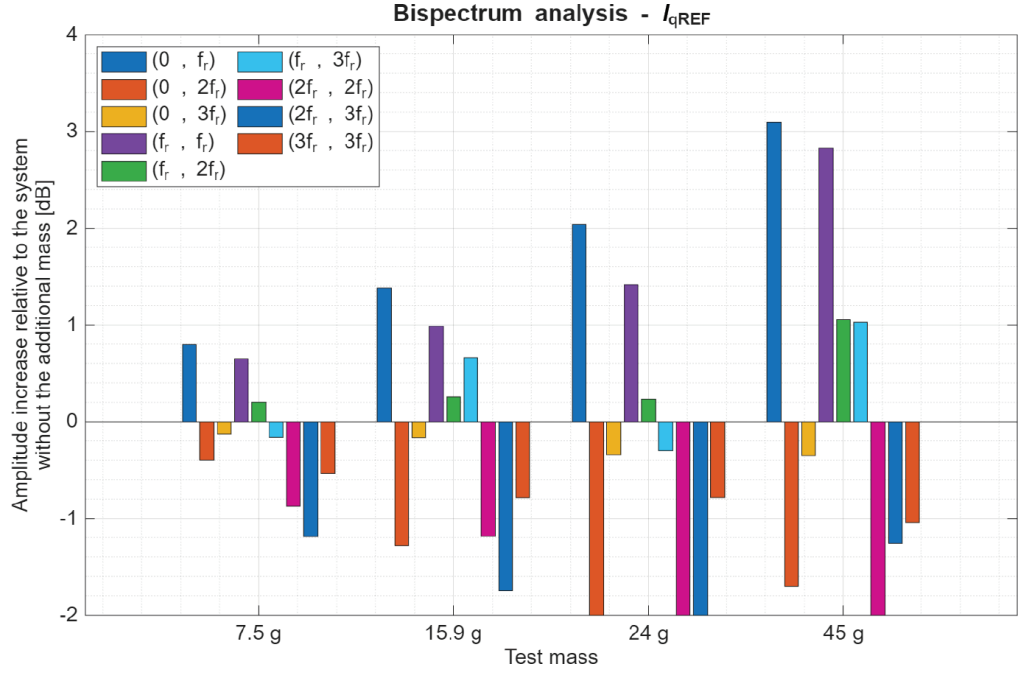

Figure 11. Summary of changes in the amplitudes of characteristic symptoms (kf_r, kf_r) derived from the bispectral analysis of the I_{qREF} current signal.

From the bispectrum analysis, two symptoms can be used to detect rotor unbalance. Both symptoms ((0, f_r) and (f_r, f_r)), similar to the f_r frequency in the FFT analysis, respond to the addition of a 45 g test mass. The observed amplitude increases are approximately 3.1 dB and 2.8 dB, respectively.

Figure 12 shows only the positive difference in the amplitudes of the symptoms (kf_r, kf_r) obtained from the bispectrum analysis of the I_{qREF} current for the motor without an installed test mass and with an installed test mass of m = 45 g. Only the symptoms that allow detection of motor unbalance are highlighted in the figure.

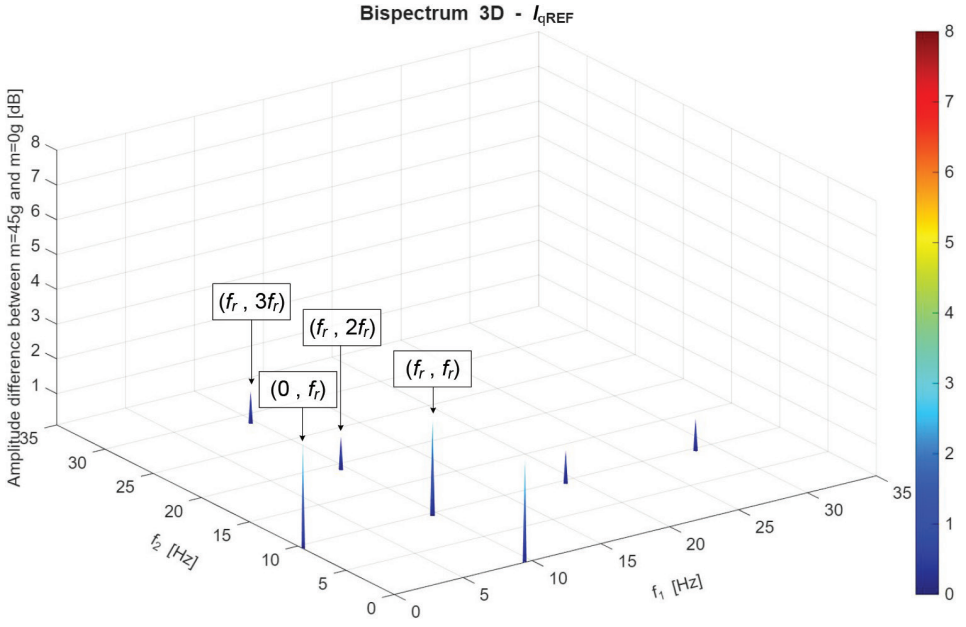

Figure 12. Difference between the amplitudes of the symptoms (kf_r, kf_r) derived from the bispectral analysis of the I_{qREF} current for the motor without an installed test mass (m = 0 g) and an installed test mass m = 45 g.

5.2. Impact of the test mass on the performance of the two-mass system

A more diagnostically challenging case concerns the two-mass system of motors connected by a long, thin shaft. Coupling the two machines introduced additional disturbances (misalignment, shaft runout, etc.), which were not identified or investigated within the scope of this article. It should be assumed that the aim of the study was to determine the symptoms that, in such a prepared (not fully identified) drive system, allow detection of rotor unbalance.

The first signal analysed was the vibration acceleration measured along the *Y*-axis. Figure 13 presents the amplitude variations of the diagnostic components in the FFT spectrum. The comparison shows that, in this case, the rotational frequency f_r is the most suitable for detecting unbalance. Adding a test mass of 45 g results in an increase in the amplitude of the rotational frequency by approximately 4.5 dB. For the $3f_r$ frequency, with test masses of 24 g and 45 g, a decrease in amplitude is observed compared to the case with a 15.9 g test mass. In both cases, the amplitudes are higher than those obtained for the drive system without an installed test mass.

The bispectrum analysis of mechanical vibration acceleration (Figure 14) shows that more symptoms can be obtained (compared to the FFT analysis) that indicate unbalance in the drive system. The most informative symptoms are: (0, f_r), (f_r, f_r), (f_r, $3f_r$), and ($2f_r$, $2f_r$). For each symptom, a clear amplitude increase is observed compared to the system without an installed test mass, amounting to approximately 4.6 dB, 5.2 dB, 13.7 dB, and 11.6 dB, respectively. Only for the (0, f_r) symptom, there is no anomaly showing a decrease in amplitude for the 24 g test mass compared to the 15.9 g case. In all analysed cases, increasing the test mass resulted in a significant increase in the amplitude of the analysed symptoms compared to those obtained for the two-mass system without an installed test mass.

Figure 15 shows only the positive difference in the amplitudes of the symptoms (kf_r, kf_r) obtained from the bispectrum analysis of vibration acceleration for the two-mass system without an installed test mass and with an installed test mass of m = 45 g.

The FFT analysis of the I_{qREF} current (Figure 16) showed that rotor unbalance in the two-mass system could only be detected starting from a test mass of 24 g. For the two smallest masses (7.5 g and 15.9 g), a reduction in the amplitude of the rotational frequency f_r was noted. It can be assumed that the thin shaft introduced asymmetry into the mechanical system, which also affected the changes observed in the I_{qREF} current. The analysis indicates that the two smallest masses had a beneficial effect on the existing asymmetry in the system. Introducing a 45 g test mass led to an increase of approximately 6.7 dB in the amplitude of the rotational frequency compared to the case without the test mass.

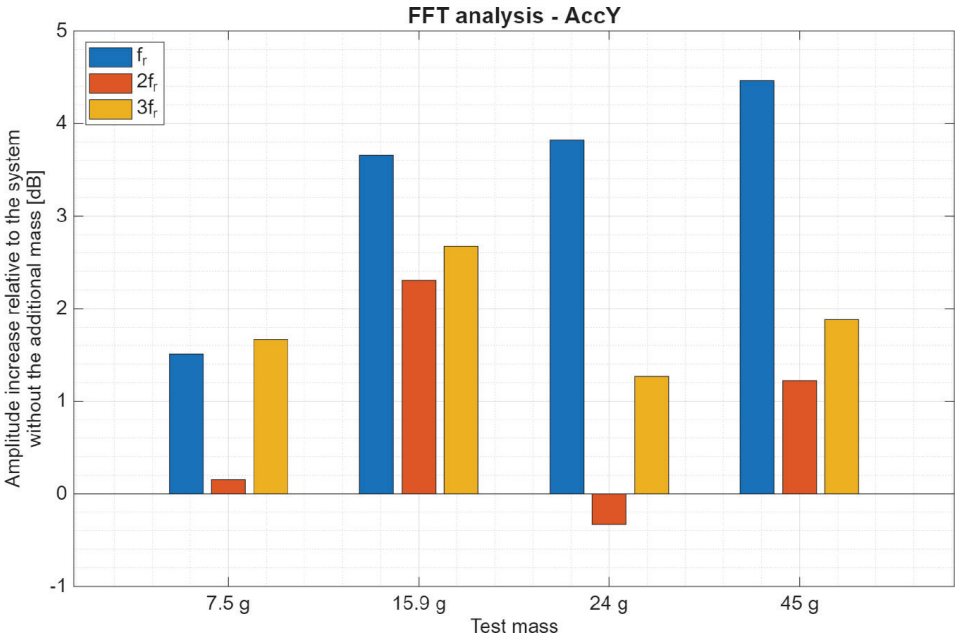

Figure 13. Summary of changes in the amplitude of kf_r symptoms derived from the spectrum of mechanical vibration acceleration.

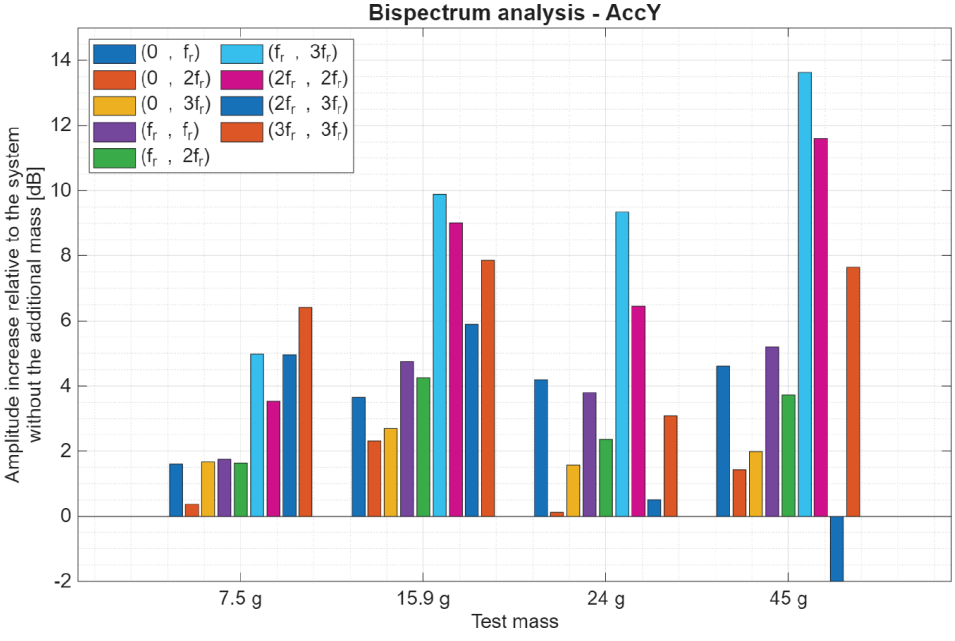

Figure 14. Summary of changes in the amplitudes of characteristic symptoms (kf_r, kf_r) derived from the bispectral analysis of mechanical vibration acceleration.

A similar phenomenon can be observed in the comparison from the bispectrum analysis (Figure 17). In this scenario, a noticeable rise in the amplitudes of the characteristic diagnostic components appears only after a 24 g test mass is applied. The symptoms useful for detecting rotor unbalance are: (0, f_r), (f_r, f_r), and (f_r, 3f_r), whose amplitudes increased by approximately 6.6 dB, 6.3 dB, and 3.6 dB, respectively.

Figure 18 shows only the positive difference in the amplitudes of the symptoms (kf_r, kf_r) obtained from the bispectrum analysis of the I_{qREF} current for the two-mass system without an installed test mass and with an installed test mass of m = 45 g.

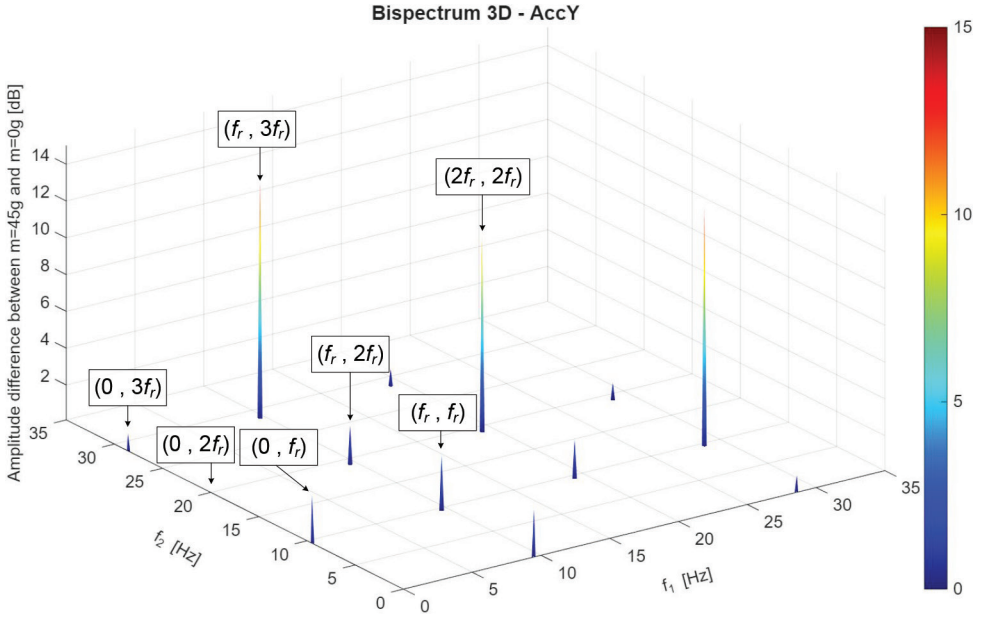

Figure 15. Difference between the amplitudes of the symptoms (kf_r, kf_r) derived from the bispectral analysis of mechanical vibration acceleration for the two-mass system without an installed test mass (m = 0 g) and an installed test mass m = 45 g.

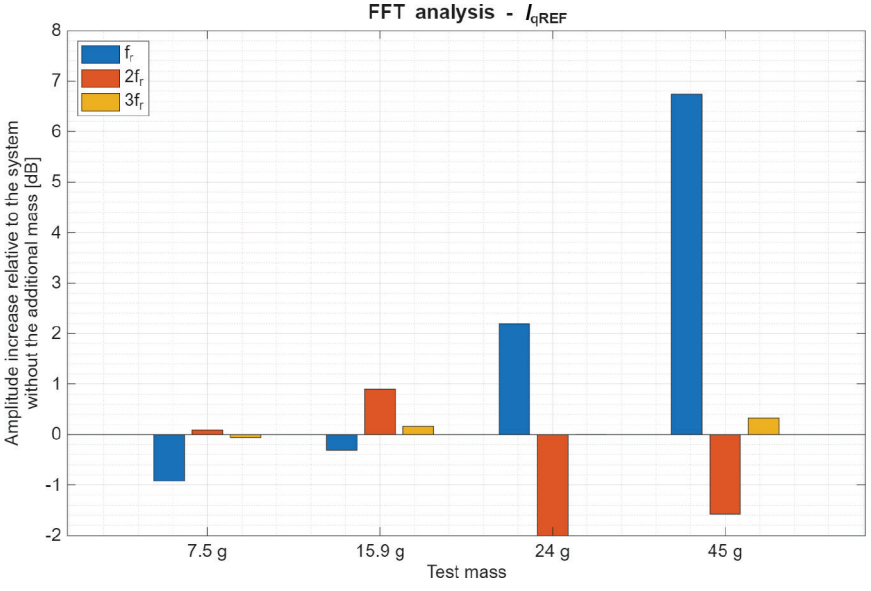

Figure 16. Summary of changes in the amplitude of kf_r symptoms derived from the spectrum of the I_{qREF} current.

5.3. Effect of rotational speed on the detectability of two-mass system unbalance

The experiments were conducted on a reassembled laboratory test bench. Following the prior disassembly and subsequent reassembly of the experimental setup, the original study was extended to include additional angular velocities. The mechanical configuration of the system does not allow for adjustment of shaft alignment, and the assembly process does not ensure reproduction of identical component positioning and stress conditions as in the previous measurement session. Consequently, it should be assumed that the mechanical properties of the system (including joint stiffness, misalignment, and unbalance) may have changed, thereby affecting the dynamic characteristics and the obtained measurement results.

As part of the extended tests, mechanical vibrations were measured using a three-axis DeltaTron 4506 B 003 accelerometer manufactured by Brüel & Kjaer, mounted on the motor's mounting bracket. The sensor exhibited a

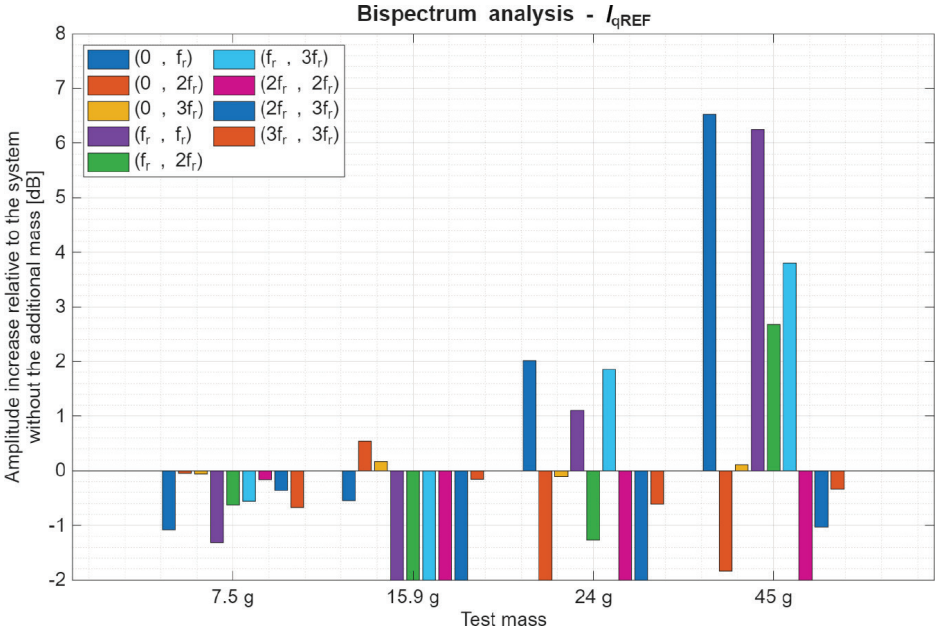

Figure 17. Summary of changes in the amplitudes of characteristic symptoms (kf_r, kf_r) derived from the bispectral analysis of the I_{qREF} current signal.

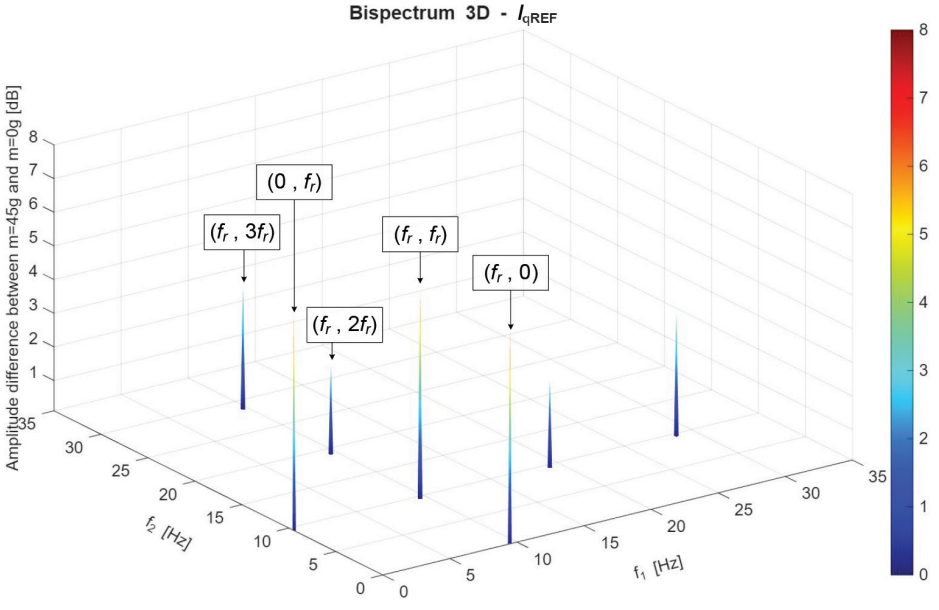

Figure 18. Difference between the amplitudes of the symptoms (kf_r, kf_r) derived from the bispectral analysis of the I_{qREF} current for a two-mass system without an installed test mass (m = 0 g) and an installed test mass m = 45 g.

sensitivity five times greater than that of the accelerometer used in the original measurements. The reference current (I_{qREF}) and mechanical vibrations were acquired using the NI USB-9234 acquisition card from National Instruments. All signals were acquired over a duration of 10 s with a sampling frequency of 3.2 kS/s, which was four times lower than the sampling frequency applied during the original experimental study. The I_{qREF} signal was generated by a vector control system implemented on the super harvard architecture computer (SHARC) DSP 26369 digital signal processor manufactured by Analog Devices. The motor was supplied by a laboratory three-phase power converter.

The reanalysed signals were subsequently resampled to 200 S/s. Rotor unbalance was modelled using eight test masses: 6 g, 16 g, 25 g, 36 g, 46 g, 56 g, 72 g, and 93 g. The investigated drive system operated under no-load conditions at constant angular speeds of 10 rad/s, 60 rad/s, 90 rad/s, 110 rad/s, and 140 rad/s, respectively. FFT

and bispectral analyses were performed on the mechanical vibration acceleration signal measured along the Y-axis (AccY – Figure 19) and on the reference current signal (Figure 20).

The analysis of Figure 19 demonstrated that the unbalance symptoms identified in Section 5.2 of this paper, obtained from FFT and bispectral analyses of mechanical vibrations, enable successful detection of unbalance in the investigated two-mass system with a flexible coupling over the extended range of angular velocities and test masses. Difficulties were observed only at the angular velocity of 10 rad/s, which may be too low to generate a sufficiently large centrifugal force. Furthermore, it can be observed that the amplitudes of the analysed symptoms increase with increasing angular velocity.

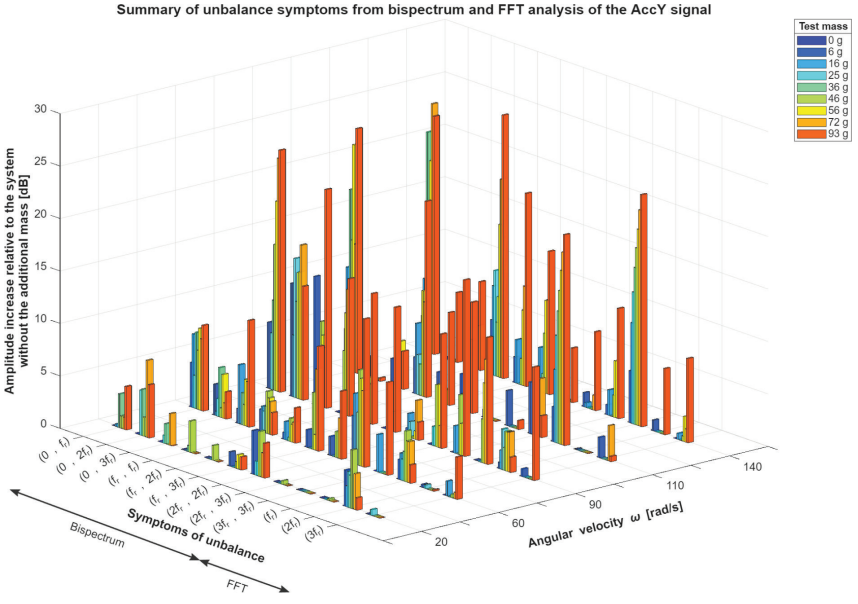

Figure 19. Summary of changes in the amplitudes of characteristic symptoms (kf_r, kf_r) derived from the bispectral analysis and kf_r derived from the FFT analysis of mechanical vibration acceleration.

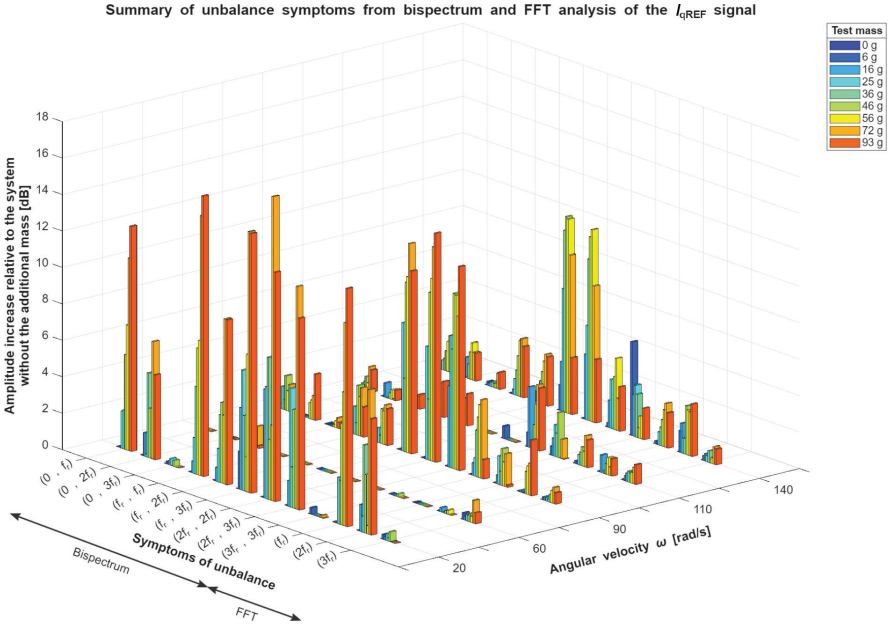

Figure 20. Summary of changes in the amplitudes of characteristic symptoms (kf_r, kf_r) derived from the bispectral analysis and kf_r derived from the FFT analysis of the I_{qREF} current signal.

The analysis of the I_{qREF} signal (Figure 20) showed that it is possible to detect unbalance in the two-mass system even at low angular speeds of approximately 10 rad/s. However, in this case, no increase in the amplitude difference between the condition with an additional test mass and the condition without the additional mass was observed with increasing rotational speed. This is due to the fact that the centrifugal force does not affect the operation of the control system. From the controller perspective, the dominant factors remain the torques generated by gravitational forces coming from additional mass, as well as friction torques in the bearings and structural stress-related torques affecting the rotational motion.

6. Summary

Unbalance of rotating components adversely affects the entire drive system. Unfortunately, there are no instruments that allow direct measurement of imbalance during operation, making it necessary to measure the secondary effects of mechanical asymmetry.

This article introduced a method for identifying rotor unbalance in a two-mass system connected by an elastic coupling. The proposed approach combines FFT analysis with bispectral examination of mechanical vibration acceleration and the I_{qREF} current signal from the control system. It was shown that using a higher-order transform, such as bispectrum analysis, increases the number of symptoms characteristic of unbalance. A greater number of symptoms should positively impact the effectiveness of unbalance detection.

Bispectrum analysis provides a 2–-3 times higher increase in the amplitude of characteristic frequencies compared to an equivalent comparison based on FFT of mechanical vibrations. For the I_{qREF} current, changes in the amplitudes of the analysed symptoms are at a similar level. Using the I_{qREF} current to detect drive system imbalance does not require additional external measurement sensors and can be implemented directly in a signal processor.

A disadvantage of bispectrum analysis compared to classical FFT analysis is its computational complexity, which results in longer processing times. This issue can be mitigated by reducing the sampling rate of the analysed signal, as demonstrated in the article.

The proposed diagnostic methods allow detection of rotor unbalance in a single-mass system caused by a small test mass of 7.5 g, which corresponds to approximately 0.22% of the rotor mass. For the two-mass system, using mechanical vibration signals enables detection of unbalance caused by a similar test mass, corresponding to about 0.085% of the rotating elements' mass. Analysis of the I_{qREF} current allows detection of unbalance caused by a 24 g test mass, or approximately 0.27% of the rotating elements' mass in the two-mass system. These values were obtained at an angular velocity of 60 rad/s, corresponding to about 19% of the nominal speed.

The proposed signal processing methods for vibration acceleration and I_{qREF} current allow effective detection of rotor unbalance in both single-and two-mass systems at an early stage. The detection process does not require high sampling frequencies; for a system rotating at 60 rad/s, a sampling rate of 200 S/s provides sufficient accuracy.

To improve the effectiveness of unbalance detection in a two-mass system with a flexible coupling over a wide range of angular speeds and for small unbalance-inducing masses (approximately 0.085% of the mass of the rotating components), simultaneous analysis of the I_{qREF} signal and mechanical vibrations is recommended.

Acknowledgment

The research reported in this publication was conducted within the framework of a grant funded by the National Science Centre, Poland: Step Towards Self-Aware Electric Drives, 2024/53/B/ST7/01308.

References

AbdulBary, M., Embaby, A. and Gomaa, F. (2021). Fault Diagnosis in Rotating System Based on Vibration Analysis. *Engineering Research Journal (ERJ)*, 44(3), pp. 285–294. doi: 10.21608/erjm.2021.61436.1080

Argenti, F., Nesi, P. and Pantaleo, G. (2011). Automatic Transcription of Polyphonic Music Based on the Constant-Q Bispectral Analysis. *IEEE Transactions on Audio, Speech, and Language Processing*, 19(6), pp. 1610–1630. doi: 10.1109/TASL.2010.2093894

Boudiaf, M., Cherroun, L. and Benbrika, M. (2018). Real-Time Diagnosis of Three-Phase Induction

Machine Using Arduino-Uno Card Based on Park's Circle Method. *Diagnostyka*, 19(3), pp. 63–71. doi: 10.29354/diag/90641

Calderon-Uribe, U., Lizarraga-Morales, R. A. and Guryev, I. V. (2023). Unbalance Detection in Induction Motors Through Vibration Signals Using Texture Features. *Applied Sciences*, 13(10), p. 6137. doi: 10.3390/app13106137

Chen, Y., Liang, S., Li, W., Liang, H. and Wang, C. (2019). Faults and Diagnosis Methods of Permanent Magnet Synchronous Motors: A Review. *Applied Sciences*, 9(10), p. 2116. doi: 10.3390/app9102116

Diversi, R., Lenzi, A., Speciale, N. and Barbieri, M. (2025). An Autoregressive-Based Motor Current Signature Analysis Approach for Fault Diagnosis of Electric Motor-Driven Mechanisms. *Sensors*, 25(4), p. 1130. doi: 10.3390/s25041130

Dogan, Z. and Tetik, K. (2021). Diagnosis of Inter-Turn Faults Based on Fault Harmonic Component Tracking in LSPMSMs Working Under Nonstationary Conditions. *IEEE Access*, 9, pp. 92101–92112. doi: 10.1109/ACCESS.2021.3092605

Ebrahimi, B. J., Faiz, J. and Roshtkhari, M. J. (2009). Static-, Dynamic-, and Mixed-Eccentricity Fault Diagnoses in Permanent-Magnet Synchronous Motors. *IEEE Transactions on Industrial Electronics*, 56(11), pp. 4727–4739. doi: 10.1109/TIE.2009.2029577

Ewert, P. (2020). The Application of the Bispectrum Analysis to Detect the Rotor Unbalance of the Induction Motor Supplied by the Mains and Frequency Converter. *Energies*, 13(11), p. 3009. doi: 10.3390/en13113009

Ewert, P., Kowalski, C. T. and Jaworski, M. (2022). Comparison of the Effectiveness of Selected Vibration Signal Analysis Methods in the Rotor Unbalance Detection of PMSM Drive System. *Electronics*, 11(11), p. 1748. doi: 10.3390/electronics11111748

Ewert, P., Kowalski, C. T. and Orlowska-Kowalska, T. (2020). Low-Cost Monitoring and Diagnosis System for Rolling Bearing Faults of the Induction Motor Based on Neural Network Approach. *Electronics*, 9(9), p. 1334. doi: 10.3390/electronics9091334

Ewert, P., Pajchrowski, T. and Wicher, B. (2024). Sensorless Detection of Mechanical Unbalance in Servodrive with Elastic Coupling. *Energies*, 17(19), p. 4859. doi: 10.3390/en17194859

Faiz, J., Takbash, A. M. and Mazaheri-Tehrani, E. (2017). Application of Signal Processing Tools for Fault Diagnosis in Induction Motors—A Review—Part I. *AUT Journal of Electrical Engineering*, 49(2), pp. 109–122. doi: 10.22060/eej.2017.13219.5142

Hachemi Benbouzid, M. E. (2000). A Review of Induction Motors Signature Analysis as a Medium for Faults Detection. *IEEE Transactions on Industrial Electronics*, 47(5), pp. 984–993. doi: 10.1109/41.873206

Jia, N., Cheng, Y., Liu, Y. and Tian, Y. (2022). Intelligent Fault Diagnosis of Rotating Machines Based on Wavelet Time–Frequency Diagram and Optimized Stacked Denoising Auto-Encoder. *IEEE Sensors Journal*, 22(17), pp. 17139–17150. doi: 10.1109/JSEN.2022.3193943

Kim, H. (2009). On-Line Mechanical Unbalance Estimation for Permanent Magnet Synchronous Machine Drives. *IET Electric Power Applications*, 3(3), pp. 178–186. doi: 10.1049/iet-epa.2008.0078

Korkua, S., Jain, H., Lee, W.-J. and Kwan, C. (2010). Wireless health monitoring system for vibration detection of induction motors. In: *IEEE Industrial and Commercial Power Systems Technical Conference*. doi: 10.1109/ICPS.2010.5489899.

Krichen, M., Benhadj, N., Chaeib, M. and Neji, R. (2017). Fault detection and diagnosis methods in permanent magnet synchronous machines: A review. In: International Conference on Recent Advances in Electrical Systems, pp. 229–237. Available at: https://www.researchgate.net/publication/328610743_Fault_Detection_and_Diagnosis_Methods_in_Permanent_Magnet_Synchronous_Machines_A_Review [Accessed 11 May 2026]

Liang, H., Chen, Y., Liang, S. and Wang, C. (2018). Fault Detection of Stator Inter-Turn Short-Circuit in PMSM on Stator Current and Vibration Signal. *Applied Sciences*, 8(9), p. 1677. doi: 10.3390/app8091677

Łuczak, D. (2024). Machine Fault Diagnosis Through Vibration Analysis: Continuous Wavelet Transform With Complex Morlet Wavelet and Time–Frequency RGB Image Recognition via Convolutional Neural Network. *Electronics*, 13(2), p. 452. doi: 10.3390/electronics13020452

Matsuoka, T. and Ulrych, T. J. (1984). Phase Estimation Using the Bispectrum. *Proceedings of the IEEE*, 72(10), pp. 1403–1411. doi: 10.1109/PROC.1984.13027

Nandi, S., Toliyat, H. A. and Li, X. (2005). Condition Monitoring and Fault Diagnosis of Electrical Motors—A Review. *IEEE Transactions on Energy Conversion*, 20(4), pp. 719–729. doi: 10.1109/TEC.2005.847955

Niu, G., Dong, X. and Chen, Y. (2023). Motor Fault Diagnostics Based on Current Signatures: A Review. *IEEE Transactions on Instrumentation and Measurement*, 72, pp. 1–19. doi: 10.1109/TIM.2023.3285999

Orhan, A., Yordanov, N., Ertarğın, M., Zhilevski, M. and Mikhov, M. (2025). A Comparative Study of Time–Frequency Representations for Bearing and Rotating Fault Diagnosis Using Vision Transformer. *Machines*, 13(8), p. 737. doi: 10.3390/machines13080737

Orlowska-Kowalska, T., Wolkiewicz, M., Pietrzak, P., Skowron, M., Ewert, P., Tarchala, G., Krzysztofiak, M. and Kowalski, C. T. (2022). Fault Diagnosis and Fault-Tolerant Control of PMSM Drives—State of the Art and Future Challenges. *IEEE Access*, 10, pp. 59979–60024. doi: 10.1109/ACCESS.2022.3180153

Rahman, M. M. and Uddin, M. N. (2017). Online Unbalanced Rotor Fault Detection of an IM Drive Based on Both Time and Frequency Domain Analyses. *IEEE Transactions on Industry Applications*, 53(4), pp. 4087–4096. doi: 10.1109/TIA.2017.2691736

Ribeiro Junior, R. F., De Almeida, F. A. and Gomes, G. F. (2020b). Fault Classification in Three-Phase Motors Based on Vibration Signal Analysis and Artificial Neural Networks. *Neural Computing and Applications*, 32(18), pp. 15171–15189. doi: 10.1007/s00521-020-04868-w

Ruqiang, Y., Robert, X. G. and Xuefeng, C. (2014). Wavelets for Fault Diagnosis of Rotary Machines: A Review With Applications. *Signal Processing*, 96(Part A), pp. 1–15. doi: 10.1016/j.sigpro.2013.04.015

Schmidt, O. T. (2020). Bispectral Mode Decomposition of Nonlinear Flows. *Nonlinear Dynamics*, 102, pp. 2479–2501. doi: 10.1007/s11071-020-06037-z

Sergakis, A., Salinas, M., Gkiolekas, N. and Gyftakis, K. N. (2025). A Review of Condition Monitoring of Permanent Magnet Synchronous Machines: Techniques, Challenges and Future Directions. *Energies*, 18(5), p. 1177. doi: 10.3390/en18051177

Sun, L., Feng, Z., Lu, N., Wang, B. and Zhang, W. (2019). An Advanced Bispectrum Features for EEG-Based Motor Imagery Classification. *Expert Systems with Applications*, 131, pp. 9–19. doi: 10.1016/j.eswa.2019.04.021

Thang, J., Yang, Y., Chen, J., Qiu, R. and Liu, Z. (2020). Characteristics Analysis and Measurement of Inverter-Fed Induction Motors for Stator and Rotor Fault Detection. *Energies*, 13(1), p. 101. doi: 10.3390/en13010101

Thomson, W. T. and Fenger, M. (2001). Current Signature Analysis to Detect Induction Motor Faults. *IEEE Industry Applications Magazine*, 7(4), pp. 26–34. doi: 10.1109/2943.930988

Tiboni, M., Remino, C., Bussola, R. and Amici, C. (2022). A Review on Vibration-Based Condition Monitoring of Rotating Machinery. *Applied Sciences*, 12(3), p. 972. doi: 10.3390/app12030972

Tran, M.-Q., Liu, M.-K., Tran, Q.-V. and Nguyen, T.-K. (2022). Effective Fault Diagnosis Based on Wavelet and Convolutional Attention Neural Network for Induction Motors. *IEEE Transactions on Instrumentation and Measurement*, 71, pp. 1–13. doi: 10.1109/TIM.2021.3139706

Wang, Z., Yang, J., Ye, H. and Zhou, W. (2014). A review of permanent magnet synchronous motor fault diagnosis. In: *IEEE Conference and Expo Transportation Electrification Asia-Pacific*. doi: 10.1109/ITEC-AP.2014.6940870.

Wicher, B. and Nowopolski, K. (2017). Model of ADRC speed control system for complex mechanical object with backlash. In: *22nd International Conference on Methods and Models in Automation and Robotics*, Miedzyzdroje, Poland 2017, pp. 379–383. doi: 10.1109/MMAR.2017.8046857.

Wolkiewicz, M. and Skowron, M. (2017). Diagnostic System for Induction Motor Stator Winding Faults Based on Axial Flux. *Power Electronics and Drives*, 2(2), pp. 137–150. doi: 10.5277/PED170204

Yamamoto, G. K., Da Costa, C. and Sousa, J. S. (2016). A Smart Experimental Setup for Vibration Measurement and Imbalance Fault Detection in Rotating Machinery. *Case Studies in Mechanical Systems and Signal Processing*, 4, pp. 8–18. doi: 10.1016/j.csmssp.2016.07.001

Yatsugi, K., Pandarakone, S. E., Mizuno, Y. and Nakamura, H. (2023). Common Diagnosis Approach to Three-Class Induction Motor Faults Using Stator Current Feature and Support Vector Machine. *IEEE Access*, 11, pp. 24945–24952. doi: 10.1109/ACCESS.2023.3254914

Zhang, Y. and Wang, L. (2019). Entropy-Based Methods for Fault Diagnosis of Electric Machines. *Sensors*, 19(15), p. 3401. doi: 10.3390/s19153401